Unidirectional self-transport of air bubble via a Janus membrane in aqueous environment

Cite as: Appl. Phys. Lett. **113**, 261602 (2018); https://doi.org/10.1063/1.5052566
Submitted: 20 August 2018 . Accepted: 04 December 2018 . Published Online: 27 December 2018

Shuguang Yan, Feifei Ren, Chuanzong Li, Yunlong Jiao, Chaowei Wang, Sizhu Wu, Sui Wei, Yanlei Hu, Jiawen Li, Yi Xiao, Yahui Su, and Dong Wu

Unidirectional self-transport of air bubble via a Janus membrane in aqueous environment

Shuguang Yan,[1,a)] Feifei Ren,[1,a)] Chuanzong Li,[2] Yunlong Jiao,[3] Chaowei Wang,[3] Sizhu Wu,[2] Sui Wei,[4] Yanlei Hu,[3] Jiawen Li,[3] Yi Xiao,[5] Yahui Su,[1,4,b)] and Dong Wu[3,b)]
[1]*School of Electrical Engineering and Automation, Anhui University, Hefei, Anhui 230601, People's Republic of China*
[2]*School of Instrument Science and Opto-electronics Engineering, Hefei University of Technology, Hefei, Anhui 230009, People's Republic of China*
[3]*CAS Key Laboratory of Mechanical Behavior and Design of Materials, Department of Precision Machinery and Precision Instrumentation, University of Science and Technology of China, Hefei, Anhui 230026, People's Republic of China*
[4]*Key Laboratory of Computational Intelligence and Signal Processing, Ministry of Education, Anhui University, Hefei, Anhui 230039, People's Republic of China*
[5]*School of Mechanical Engineering, Nantong Vocational University, Nantong, Jiangsu 226007, People's Republic of China*

(Received 20 August 2018; accepted 4 December 2018; published online 27 December 2018)

Inspired by natural creatures, bubble manipulation by surface microstructures in aqueous media has attracted great attention due to its promising applications in industrial production. Herein, a superhydrophobic/hydrophilic Janus aluminum membrane with tapered micropore arrays was fabricated by femtosecond laser drilling, surface fluorination, and subsequent fluorination removal. Compared with the single interception or penetration of double-faced hydrophilic or superhydrophobic membranes, the Janus membrane showed a distinctive unidirectional air bubble transport ability. In experiment, the air bubbles introduced on the lower hydrophilic surface could spontaneously move to the upper superhydrophobic surface, but they were prevented in the inverse direction. The dynamic process of unidirectional transport was *in-situ* monitored, and the physical mechanism was systemically investigated. In addition, the concepts of air-participating chemical/physical processes were demonstrated such as discoloration of purple litmus solution by CO_2 injection, which proved the Janus membrane practicability. *Published by AIP Publishing.*
https://doi.org/10.1063/1.5052566

In recent years, bubble manipulation by special wettability has attracted great attention due to its promising applications in the aeration process, water treatment, etc.[1,2] Air bubbles in the aqueous environment could bring about serious corrosion and blockage, and the high impact pressure produced by cavitation bubbles can destroy the surface of solid materials.[3–5] It is of great significance to achieve controllable bubble manipulation in the aqueous environment.

In the structures of spider silk[6] and cactus spine,[7] water droplets are effectively captured and directionally transported. One of the main factors is that they contain tapered microstructures, which lead to the self-driving Laplace pressure.[8] Another factor is that the gradient of the surface free energy arising from the gradient chemical modification guarantees quick transport of the drops.[9] Similarly, the Laplace pressure and the gradient of the surface free energy were expected to control the behavior of the air bubble in the aqueous environment.[10–12] Xue *et al*. reported the cone structure with the surface free energy gradient fabricated by gradient electrochemical corrosion and achieved spontaneous and directional underwater bubble transport.[11]

It is well-known that a type of Janus membrane with asymmetrical wettability can transport water directionally.[13–17] On one side, its wetting is superhydrophobic while the wetting on the other side is superhydrophilic. The droplet can easily pass through it from the superhydrophobic side to the superhydrophilic side; however, opposite directional water transport is blocked. This is attributed to the generation of a wettability gradient from one side to the other. On the basis of this design strategy, researchers have prepared Janus membranes with unidirectional droplet transport properties for controllable water behavior.[13–15,18,19] Similarly, the Janus membrane is capable of continuously and unidirectionally transporting air bubbles underwater. Chen *et al*. fabricated a superhydrophobic/hydrophilic Janus mesh via a facile single-face coating process with the assistance of liquid surface tension and UV degradation for an underwater air "diode."[20] However, this method is based on the commercial stainless steel mesh with additional nanoparticle coating and UV irradiation; thus, it is uncontrollable for the size and shape of the pores and not suitable for various materials.

Femtosecond laser drilling is a powerful method which can be widely employed to fabricate micropore arrays covered with micro/nanostructures due to its high precision, excellent controllability, and wide compatiblity with various materials.[21] Herein, a strategy that imitates nature is proposed for air bubble unidirectional transport underwater through the employment of the superhydrophobic/hydrophilic Janus aluminum membrane. This Janus membrane was fabricated by femtosecond laser drilling, surface fluorination, and subsequent fluorination removal. The air bubble

[a)]S. Yan and F. Ren contributed equally to this work.
[b)]E-mail: ustcsyh@ahu.edu.cn and dongwu@ustc.edu.cn

showed different movements on different sides of the Janus membrane. In addition, due to the gradient of the surface energy, a self-driving force was produced from the hydrophilic surface to the superhydrophobic surface. The concepts of air-participating chemical/physical processes were demonstrated such as discoloration of purple litmus solution by CO_2 injection. This study provides deep insights into the asymmetric membrane with unique ability, which will be beneficial for their practical applications.

Figure 1(a) shows the typical fabrication process of the Janus membrane, which can be divided into three steps. First, high-uniformity micropore arrays were fabricated by femtosecond laser micro-drilling.[21–25] Then, the double-faced superhydrophilic aluminum foil was modified by low surface energy fluorosilane, and the sample turned into double-faced superhydrophobicity. Subsequently, Janus aluminum foil was obtained by laser scanning to remove a part of the PFDTES-modified material on the bottom surface. The as-prepared aluminum foil exhibited a significant morphologic difference between its two sides. The mastoids around the pore would produce microscaled roughness on the bottom surface [Fig. 1(b)], whereas the top surface is relatively more smooth [Fig. 1(c)]. The bottom surface of the Janus membrane is hydrophilic with a water contact angle (WCA) of ∼23° [Fig. 1(d)] and aerophobic underwater with a bubble contact angle (BCA) of ∼118° [Fig. 1(e)] due to the removal of the PFDTES-modified material. On the contrary, laser scanning would not damage the top surface, and the modified material was facilitated with superhydrophobicity. As shown in Fig. 1(f), the WCA on the top surface is as high

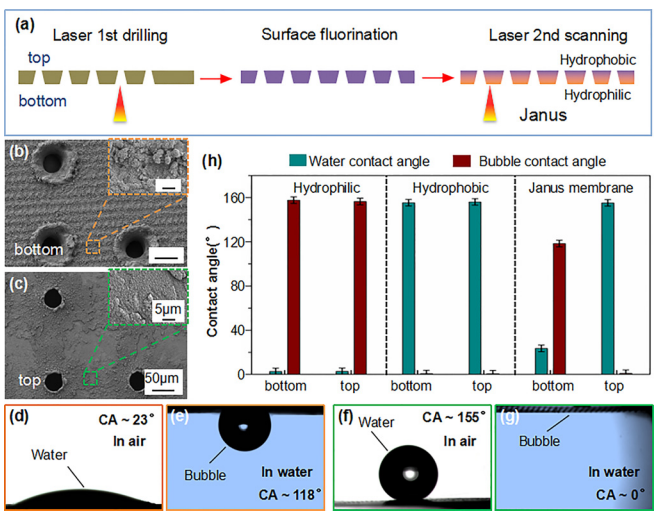

FIG. 1. Fabrication of the Janus membrane with tapered micropore arrays. (a) Schematic illustration of the preparation process of the Janus membrane fabricated by femtosecond laser micro-drilling, surface modification with fluorosilane, and laser scanning on the bottom surface. (b) and (c) SEM image of the fabricated bottom and top surfaces with micropore arrays and the inset is its magnified SEM image which shows that the fabricated surface is facilitated with the micro/nanostructures. (d) and (e) The WCA and the BCA on the fabricated bottom surface of the Janus membrane, which demonstrate that it is hydrophilic with a water contact angle (WCA) of ∼23° and aerophobic underwater with a bubble contact angle (BCA) of ∼118°. (f) and (g) The WCA and the BCA on the fabricated top surface of the Janus membrane, which demonstrate that it is superhydrophobic in air and superaerophilic in underwater. (h) The water contact angles in air and bubble contact angles underwater on each surface of the double-faced hydrophilic, double-faced hydrophobic, and Janus membranes.

as 155°, and it demonstrates lower adhesive force to water with a sliding angle (SA) of ∼5°. Underwater, the superhydrophobic surface is superaerophilic, where the air bubble will rapidly spread and develop into a thin air film, and the BCA was ∼0° [Fig. 1(g)]. As a comparison, we also compared the water contact angles in air and bubble contact angles underwater on each surface of the double-faced hydrophilic and double-faced hydrophobic membranes. The data were summarized as shown in Fig. 1(h).

The micropore morphology of the Janus membrane was investigated. From the scanning electron microscopy pictures in Figs. 2(a) and 2(b), it is seen that the bottom diameter (∼54.6 μm) is larger than the top diameter (∼41.9 μm). The tapered morphology of the micropores is caused by the lens focusing characteristics of an elliptical ball-shaped focused laser spot and Gaussian power distribution [Fig. 2(c)]. It can be seen that the cauliflower-like big protrusions are randomly distributed on the lower area, and the protuberance on the upper area is relatively small as shown in the insets. The surface chemical compositions were further investigated by using EDS [Figs. 2(d) and 2(e)]. The result showed nearly no signal of and mass of fluorine on the bottom and top surfaces, indicating that laser scanning has almost damaged the PFDTES-modified material at the bottom surface. The remarkable difference in the chemical composition and surface roughness contributes to the wettability diversity of the Janus membrane. The phenomenon that the air bubble would transport toward the inner-tapered pore and transfer to the opposite surface can be explained by the wettability difference.

In general, the original wetting nature of the material surface could be amplified by the roughness, according to Wenzel's law

$$\cos\theta_{bubble} = r\cos\theta'_{bubble}, \tag{1}$$

where r represents the roughness, and θ'_{bubble} and θ_{bubble} are the bubble contact angles of underwater setting on flat and rough substrates, respectively. For the bottom surface of the Janus membrane, it is more hydrophilic and aerophobic underwater, whereas the top is more hydrophobic and aerophilic underwater. Both the bottom and top surfaces are at the Wenzel state for air bubble underwater (Fig. S1, supplementary material). By comparison, the wettability inside the tapered micropore is quite complex. There is a gradient of the residual PFDTES-modified material caused by the difference of laser energy along the optical axis direction. It is shown in Fig. S2 (supplementary material) that the content of fluorine gradually decreases from the upper area to the lower area of the inner tapered pore. In addition, the microstructure in the inner pore is able to amplify the wetting ability. The air bubble on tapered pores is subjected to a driving force $F_{wet\text{-}force}$ that arises from the wettability gradient. The force analysis can be described as follows:[6,7,10,22,26,27]

$$F_{wet-force} = \cos\frac{\alpha}{2}\int_{\theta_{\text{bottom}}}^{\theta_{top}} -2\pi R\gamma\sin\theta d\theta, \tag{2}$$

where α, γ, R, θ_{bottom}, and θ_{top} are the tip angle of the tapered micropore, water surface tension, the local radius of the

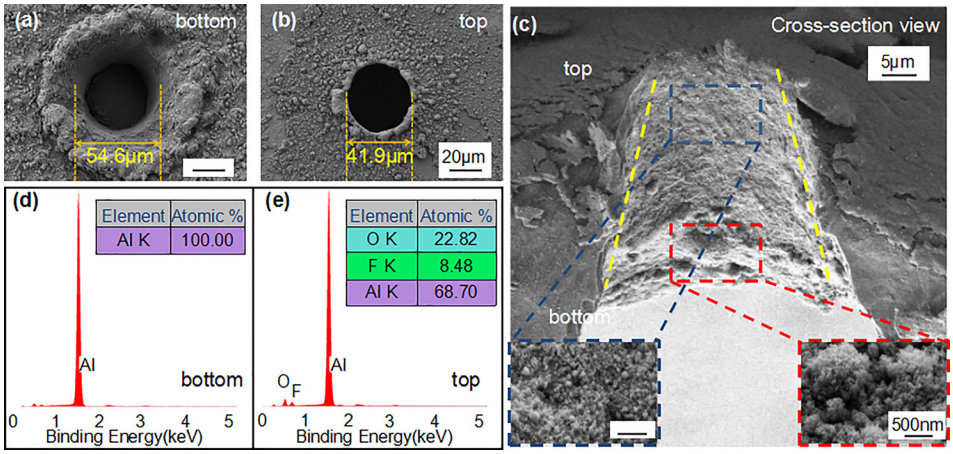

FIG. 2. (a) and (b) The SEM images of the bottom and top surfaces of the Janus membrane. (c) The cross-sectional view of a tapered pore and the inset is its magnified SEM image of upper and lower areas in the inner tapered pore. (d) and (e) the EDS elemental analysis on the chemical compositions of the bottom and top surfaces of the Janus membrane, respectively.

tapered micropore, and the bubble contact angles on the bottom and top of tapered micropores, respectively. The values of γ, θ_{bottom}, and θ_{top} are estimated to be 7.2×10^{-2} N/m, 118°, and 0°. R is from 27.3 to 21 μm. Hence, the wetting driving force ($F_{wet\text{-}force}$) is roughly estimated to be $\sim 1.5759 \times 10^{-5}$ N when the tapered micropore is filled with air bubbles.

The air bubble transport experiment was conducted to analyze the air bubble unidirectional transport ability of the Janus membrane, which was also compared with double-faced hydrophilic and superhydrophobic ones. The air bubbles were continuously introduced under the membrane via an air syringe in an aqueous environment. The air bubble movement on the double-faced hydrophilic membrane is illustrated in Fig. 3(a) and Movie S1, supplementary material. When the hydrophilic membrane was dipped into water, water can easily wet the micropores and both surfaces. Therefore, as the air bubbles were released underneath and contacted the membrane, all of them remained a spherical shape and could not pass through the membrane. The reason was that the water film between micropores blocked the channels. For the double-faced superhydrophobic membrane [Fig. 3(b) and Movie S2, supplementary material], a trapped air layer can be formed at both the microstructure and the tapered pore after the membrane was immersed into water. From the side view, it could be observed that the air bubbles were immediately absorbed once they contacted with the lower surface of the membrane. Subsequently, the absorbed air bubbles will penetrate toward the upper surface under the effect of buoyancy. Then, they raised above the upper surface and formed a convex air bulge. When more and more air bubbles were introduced continuously, the air bulge became bigger and bigger until the buoyancy was enough to pull bubble out of the upper surface.

Comparatively, the air bubble demonstrated a unique behavior on the Janus membrane in an aqueous environment. When the superhydrophobic surface was placed upwards [Fig. 3(c) and Movie S3, supplementary material], it can be seen that the air bubble maintained a relatively spherical shape after contacting with the lower hydrophilic surface. Then, the lower air bubble would pass through the micropores and transport upwards which remains in an aerophobic state in the whole process [Fig. S3, supplementary material]. The subsequent bubble movement was the same as that in the double-faced superhydrophobic membrane. The transported air bubble formed a convex air bulge on the upper surface and finally left in the form of a big bubble. On the contrary, when the hydrophilic surface was placed upwards, the air bubble rose up and touched the lower surface, and it would completely spread on the superhydrophobic surface, coinciding well with the double-faced superhydrophobic membrane. However, the air bubbles were inclined to stop at the lower surface and spread

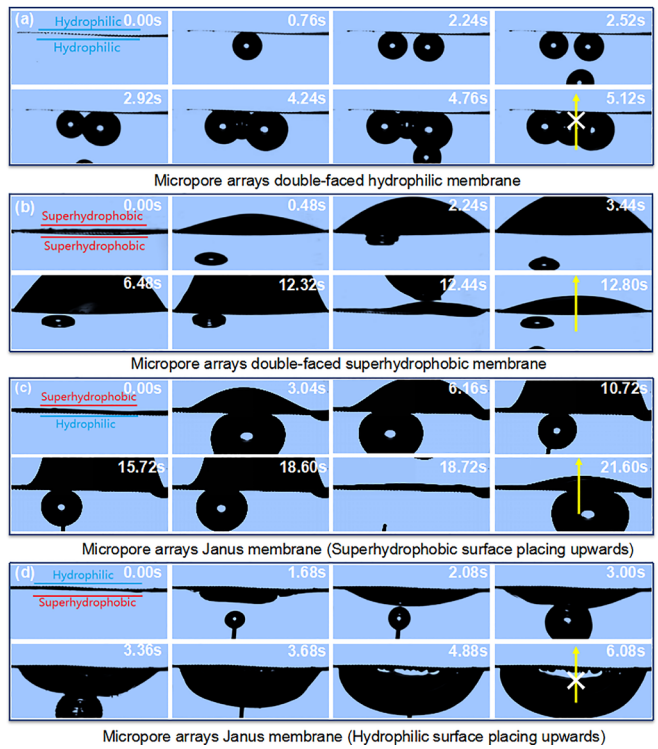

FIG. 3. *In situ* observation of air bubbles passing through the micropore array membrane. (a) The transport process of air bubbles from the lower to the upper surfaces of double-faced hydrophilic membrane is unfavorable. The air bubbles will cease at the lower surface of the hydrophilic membrane when they contacted the surface. (b) The air bubbles could pass through the double-faced superhydrophobic membrane. (c) The air bubbles could be transported from the hydrophilic surface to the superhydrophobic surface of the Janus membrane on the condition that the superhydrophobic surface was placed upwards. (d) The transport process of the air bubble from the superhydrophobic surface to the hydrophilic surface of the Janus membrane is unfavorable. The air bubble will cease at the superhydrophobic surface of the Janus membrane and spread horizontally on the condition that the hydrophilic surface was placed upwards.

horizontally [Fig. 3(d) and Movie S4, supplementary material]. In the opposite introducing direction, that is, from the superhydrophobic side to the hydrophilic side, the air bubble was intercepted by the same Janus membrane, indicating the air bubble unidirectional transport of the Janus membrane.

Furthermore, the properties of time-evolution of passing volume of air bubbles affected by the double-faced superhydrophobic membrane and the Janus membrane were also discussed, as shown in Fig. 4(a). The average passing rates of two types of membranes were 0.0259 and 0.0134 ml $s^{-1} cm^{-2}$. It can be observed that the Janus membrane has a relatively low passing rate compared with the double-faced superhydrophobic membrane. This was because air bubbles spread out completely when they contacted the lower surface of double-faced superhydrophobic membrane, and air bubbles transported only in a small part of the contact area due to its aerophobicity of the lower surface when the superhydrophobic surface was placed upwards.

The underlying mechanism resulting in these two different phenomena of the Janus membrane is shown in Figs. 4(b) and 4(c). The Laplace pressure difference of the air bubble between the upper and lower surfaces can be considered to be the basis for successful transport of the air bubble. When the superhydrophobic surface of the Janus membrane was placed upwards [Fig. 4(b)], a trapped air film would be formed between the upper superhydrophobic surface microstructure and water after the immersion. However, water can enter and completely wet the interspaces between the microstructures of the lower surface. The air bubble will remain in a spherical state while being located the lower hydrophilic surface. Then, air channels were produced through

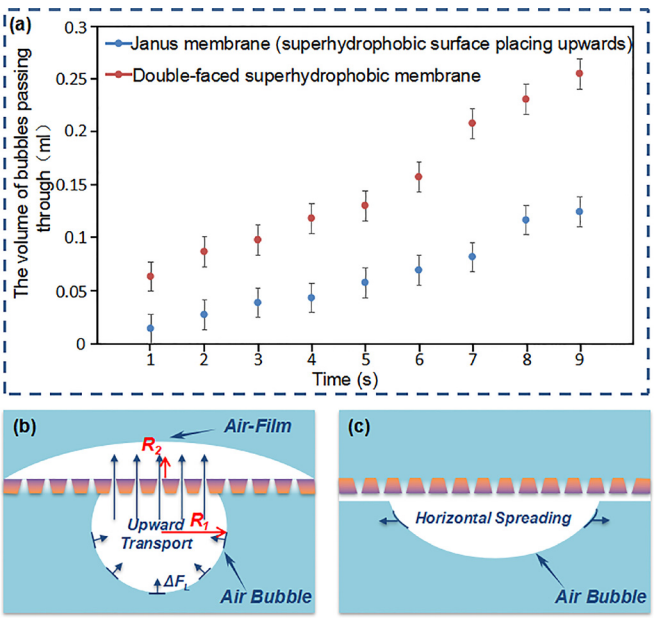

FIG. 4. (a) The passing volume (ml) with respect to the time (t) of air bubbles on the double-faced superhydrophobic membrane and the Janus membrane. (b) and (c) Schematic analysis of the transport process of the air bubble on the Janus membrane. (b) When the superhydrophobic surface was placed upwards, the air bubble can be transported from the hydrophilic surface to the superhydrophobic surface of the Janus membrane driven by the Laplace pressure difference. (c) The air bubbles were intercepted and spread horizontally owe to the air film on the lower superhydrophobic surface on the condition that the hydrophilic surface was placed upwards.

micropores from the spherical bubble to the upper air film. This is due to the difference in the radius of the air bubble (R_1) and the radius of the air film (R_2), which will produce a difference of Laplace pressure. The differential Laplace pressure (ΔF_L) can be expressed as the following equation:[7,28–31]

$$\Delta F_L = \gamma_{water}\left(\frac{1}{R_1} - \frac{1}{R_2}\right), \tag{3}$$

where γ_{water} is the surface tension of water, R_1 is the radius of curvature of the bubble, and R_2 is the radius of curvature of the air film, γ_{water} is 7.20×10^{-2} N/m, R_1 is about 840 μm, and R_2 is approaching infinity, respectively. The differential Laplace pressure (ΔF_L) is roughly estimated to be ~85.7 Pa. Due to the Laplace pressure difference between the upper air film and the lower air bubble, the air bubble will be immediately transported upwards, being coalescing with the upper air film. On the contrary, the air bubble was stopped at the lower surface instead of passing through when the hydrophilic surface was placed upwards [Fig. 4(c)]. Owing to the air film trapped on the lower superhydrophobic surface, the air bubbles can coalesce with the lower air film and then spread horizontally. Therefore, the asymmetric wettability arising from the upper and lower surfaces contributes to the unidirectional transport of the air bubble.

It is well known that the introduction of CO_2 into the water generates carbonic acid and makes the purple litmus solution red. This remarkable phenomenon was used to verify the ability of air bubble unidirectional transport of different membranes. The experimental details were designed as shown in Fig. 5 and Movie S5 (supplementary material), and the membrane was fixed between the litmus solution and the air outlet. For the double-faced hydrophilic membrane [Fig. 5(a)], the purple litmus solution failed to discolor after CO_2 injection, and the liquid environment was still neutral. For

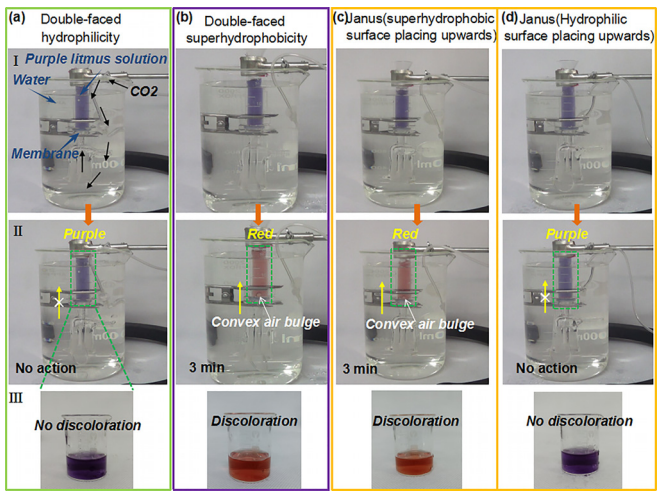

FIG. 5. Optical images of the purple litmus solution above the micropore arrays membrane discoloring after CO_2 injection. (a) The purple litmus solution above the double-faced hydrophilic membrane failed to discolor after CO_2 injection. (b) The purple litmus solution above the double-faced superhydrophobic membrane turned into red after CO_2 injection, which illustrates that the double-faced superhydrophobic membrane could realize the passage of CO_2 bubbles. (c) and (d) The purple litmus solution (c) turned into red when the superhydrophobic surface was placed upwards and (d) failed to discolor when the hydrophilic surface was placed upwards of the Janus membrane.

the double-faced superhydrophobic membrane [Fig. 5(b)], the purple litmus solution turned into red after CO_2 injection. As the convex air bulge from the white arrow, CO_2 bubbles can pass through the membrane. For the Janus membrane, when the superhydrophobic surface was placed upwards [Fig. 5(c)], CO_2 bubbles introduced into the lower surface could be transported upwards driven by the driving force and made the purple litmus solution red. It can also be observed that convex air bulge appears on upper superhydrophobic surface from the white arrow. In contrast, when the hydrophilic surface was placed upwards, the solution color did not change [Fig. 5(d)]. The litmus solutions used in experiment are shown in Figs. 5(a)(III)–5(d)(III).

A similar verification experiment was designed with chemical precipitation, as shown in Figs. S4 and S5, supplementary material. In the experiment, the purple litmus solution was replaced by $Ca(OH)_2$ and $Ba(OH)_2$ solution. The same as the former result, the turbid precipitation can be produced only in the situation of the double-faced superhydrophobic membrane and the Janus membrane with the upward superhydrophobic surface. Those series of experiment verified the unique ability of unidirectional transport and intercept, which should shed light on the development of air-involved applications.

In this paper, a superhydrophobic/hydrophilic Janus aluminum foil membrane with tapered micropores was fabricated by femtosecond laser drilling, surface fluorination, and subsequent fluorination removal. This membrane possesses the gradient of surface energy which can produce a self-driving force on the air bubble in the aqueous medium. Compared with the single interception or penetration of the double-faced hydrophilic or superhydrophobic membrane, the Janus membrane showed a distinctive unidirectional air bubble transport ability in aqueous media. In experiment, the air bubble introduced on the lower hydrophilic surface could be driven to the upper superhydrophobic surface continuously. On the opposite surface, the air bubbles were blocked. In addition, the air-participating chemical/physical processes were designed to verify the unique ability of the Janus membrane. We believe that the current finding should contribute to air-participating application underwater and can stimulate thinking in the promotion of interface science and technology.

See supplementary material for the experimental section, the dynamic process where the air bubble penetrates the Janus membrane from the hydrophilic surface to the superhydrophobic surface, the EDS elemental analysis on the chemical compositions, and air-involved applications.

This work was supported by the National Key R&D Program of China (2017YFB1104303 and 2018YFB1105400), the National Natural Science Foundation of China (Nos. 61377006, 51805508, 61505047, and 51675503), the Anhui Provincial Natural Science Foundation (No. KJ2018A0014), the China Postdoctoral Science Foundation (No. 2015M571922), and the Fundamental Research Funds for the Central Universities (WK2480000002 and WK2090090021).

[1]H. C. Yang, J. W. Hou, L. S. Wan, V. Chen, and Z. K. Xu, Adv. Mater. Interfaces **3**, 1500774 (2016).
[2]C. H. Zhang, M. Y. Cao, H. Y. Ma, C. L. Yu, K. Li, C. M. Yu, and L. Jiang, Adv. Funct. Mater. **27**, 1702020 (2017).
[3]C. A. Fairfield, Wear **317**, 92–103 (2014).
[4]S. Fontanesi, M. Giacopini, G. Cicalese, S. Sissa, and S. Fantoni, Eng. Failure Anal. **44**, 408–423 (2014).
[5]C. Reynolds and M. Yitayew, Agric. Water Manage. **29**, 25–35 (1995).
[6]Y. M. Zheng, H. Bai, Z. B. Huang, X. L. Tian, F. Q. Nie, Y. Zhao, J. Zhai, and L. Jiang, Nature **463**, 640 (2010).
[7]J. Ju, H. Bai, Y. M. Zheng, T. Y. Zhao, R. C. Fang, and L. Jiang, Nat. Commun. **3**, 1247 (2012).
[8]M. Y. Cao, J. Ju, K. Li, S. X. Dou, K. S. Liu, and L. Jiang, Adv. Funct. Mater. **24**, 3235–3240 (2014).
[9]J. Ju, K. Xiao, X. Yao, H. Bai, and L. Jiang, Adv. Mater. **25**, 5937–5942 (2013).
[10]H. Y. Ma, M. Y. Cao, C. H. Zhang, Z. L. Bei, K. Li, C. M. Yu, and L. Jiang, Adv. Funct. Mater. **28**, 1705091 (2018).
[11]X. Z. Xue, C. M. Yu, J. M. Wang, and L. Jiang, ACS Nano **10**, 10887 (2016).
[12]C. M. Yu, M. Y. Cao, Z. C. Dong, J. M. Wang, K. Li, and L. Jiang, Adv. Funct. Mater. **26**, 3236–3243 (2016).
[13]M. Y. Cao, J. S. Xiao, C. M. Yu, K. Li, and L. Jiang, Small **11**, 4379–4384 (2015).
[14]X. L. Tian, H. Jin, J. Sainio, R. H. A. Ras, and O. Ikkala, Adv. Funct. Mater. **24**, 6023–6028 (2014).
[15]H. X. Wang, J. Ding, L. M. Dai, X. G. Wang, and T. Lin, J. Mater. Chem. **20**, 7938–7940 (2010).
[16]M. B. Wu, H. C. Yang, J. J. Wang, G. P. Wu, and Z. K. Xu, ACS Appl. Mater. Interfaces **9**, 5062–5066 (2017).
[17]H. Zhou, H. X. Wang, H. T. Niu, and T. Lin, Sci. Rep. **3**, 2964 (2013).
[18]Z. X. Wang, X. B. Yang, Z. J. Cheng, Y. Y. Liu, L. Shao, and L. Jiang, Mater. Horiz. **4**, 701–708 (2017).
[19]J. Wu, N. Wang, L. Wang, H. Dong, Y. Zhao, and L. Jiang, Soft Matter **8**, 5996–5999 (2012).
[20]J. W. Chen, Y. M. Liu, D. W. Guo, M. Y. Cao, and L. Jiang, Chem. Commun. **51**, 11872–11875 (2015).
[21]S. Z. Wu, C. Z. Li, Y. L. Jiao, X. D. Lv, Z. J. Hu, G. Q. Li, J. W. Li, Y. L. Hu, J. J. Zhang, P. F. Wei, and D. Wu, Appl. Surf. Sci. **455**, 221–226 (2018).
[22]F. F. Ren, G. Q. Li, Z. Zhang, X. D. Zhang, H. Fan, C. Zhou, Y. L. Wang, Y. H. Zhang, C. W. Wang, K. Mu, Y. H. Su, and D. Wu, J. Mater. Chem. A **5**, 18403–18408 (2017).
[23]S. Ye, Q. Cao, Q. S. Wang, T. Y. Wang, and Q. Peng, Sci. Rep. **6**, 37591 (2016).
[24]C. Zhou, G. Q. Li, C. Z. Li, Z. Zhang, Y. C. Zhang, S. Z. Wu, Y. L. Hu, W. L. Zhu, J. W. Li, J. R. Chu, Z. J. Hu, D. Wu, and L. D. Yu, Appl. Phys. Lett. **111**, 141607 (2017).
[25]Z. Zhang, Y. H. Zhang, H. Fan, Y. L. Wang, C. Zhou, F. F. Ren, S. Z. Wu, G. Q. Li, Y. L. Hu, J. W. Li, D. Wu, and J. R. Chu, Nanoscale **9**, 15796–15803 (2017).
[26]M. X. Zhang, L. Wang, Y. P. Hou, W. W. Shi, S. L. Feng, and Y. M. Zheng, Adv. Mater. **27**, 5057–5062 (2015).
[27]H. Zhu, Z. G. Guo, and W. M. Liu, Chem. Commun. **52**, 3863–3879 (2016).
[28]É. Lorenceau and D. Quéré, J. Fluid Mech. **510**, 29–45 (2004).
[29]X. Y. Ma, M. Y. Cao, C. Teng, H. Li, J. S. Xiao, K. S. Liu, and L. Jiang, J. Mater. Chem. A **3**, 15540–15545 (2015).
[30]C. H. Zhang, B. Zhang, H. Y. Ma, Z. Li, X. Xiao, Y. H. Zhang, X. Y. Cui, C. M. Yu, M. Y. Cao, and L. Jiang, ACS Nano **12**, 2048–2055 (2018).
[31]C. T. Pei, Y. Peng, Y. Zhang, D. L. Tian, K. S. Liu, and L. Jiang, ACS Nano **12**, 5489–5494 (2018).